$\gamma D \rightarrow \pi^0 D$ reaction in the threshold region

M. Benmerrouche and E. Tomusiak
Department of Physics and Engineering Physics and Saskatchewan Accelerator Laboratory, University of Saskatchewan, 107 North Road, Saskatoon, Saskatchewan, Canada S7N 5C6
(Received 31 March 1998)

Coherent pion photoproduction on the deuteron is studied in the threshold region spanning photon lab energies from threshold at 139.83 MeV to 160 MeV. Unlike previous similar calculations which used the now obsolete value for the s-wave E_{0+} multipole, our work relies on the latest information on the elementary amplitudes which are in excellent agreement with recent precise data on the $\gamma p \rightarrow \pi^0 p$ reaction. We compare the exact treatment of pion propagation against various approximations often used in the literature and their impact on the very important pion rescattering contribution. We have investigated the sensitivity of the $\gamma D \rightarrow \pi^0 D$ cross section to various choices of the values of the elementary multipoles and in particular the neutron s-wave amplitude $E_{0+}^{\pi^0 n}$. The Fermi motion, corrections due to the boost from the nucleon to the deuteron frames as well as the deuteron D-state are all taken into account. The predicted total and differential cross sections are compared with the very recent experimental data from the Saskatchewan Accelerator Laboratory. [S0556-2813(98)02609-0]

PACS number(s): 25.20.Lj, 13.60.Le, 25.10.+s, 11.80.La

I. INTRODUCTION

The determination of threshold s- and p-wave amplitudes describing pion photoproduction from nucleons has recently become a topic of increased interest. It took over a decade to unambigously determine the s-wave amplitude $E_{0+}^{p\pi^0}$ from threshold π^0 photoproduction experiments on protons. The currently accepted value has been ''measured'' independently by two laboratories giving -1.32 ± 0.08 [1] and -1.31 ± 0.08 [2] in the standard units of $10^{-3}/M_{\pi^+}$ (units will be suppressed from here on). These results indicate a suppression of the cross section by nearly a factor of 4 as compared to the value anticiptated from the classical low-energy theorems (LET). A theoretical explanation based on chiral perturbation theory (ChPT) was put forward by the BKM Collaboration [3] showing that the classical LET are incomplete. There a one-loop calculation up to and including order $\mathcal{O}(q^4)$ gives $E_{0+}^{p\pi^0} = -1.16$ compared with the classical LET value of -2.47. However, an important issue regarding the convergence of the loop expansion has yet to be addressed.

A crucial question remains concerning the value for the neutron amplitude $E_{0+}^{n\pi^0}$. Theoretically, the situation for this amplitude is the reverse of what occurred for the proton. Namely, the classical LET predicts a small value of 0.5 while ChPT gives a relatively large value of 2.13, i.e., ChPT predicts 16 times more cross section than the classical LET. Unfortunately the experimental determination of $E_{0+}^{n\pi^0}$ must rely on targets with mass number greater than or equal to 2, the simplest being the deuteron. It becomes important therefore to determine the model dependence in the attempt to extract $E_{0+}^{n\pi^0}$ from the data.

Earlier investigations of coherent threshold pion production on the deuteron [4,5] have shown that the impulse approximation is not sufficient but that one must also take into account rescattering effects. That is, after being produced the pion can interact with nucleons in the deuteron. In fact the importance of this rescattering effect has been recently confirmed within the framework of ChPT. Its magnitude at threshold can be as large as six times the impulse contribution [6]. While ChPT is now believed to be the proper framework for pion-nucleon and pion-nuclei processes, it is a nontrivial task to apply it above threshold and in particular to few-body systems. Moreover, one must also understand the energy dependence of the multipoles as one deviates from threshold. For example, the strong energy dependence in the $E_{0+}^{p\pi^0}$ amplitude has a cusplike structure [7] which can only be observed as the charged pion production threshold is crossed. A similar effect should be seen in the $E_{0+}^{n\pi^0}$ amplitude and could be even more pronouced if this amplitude is as large as predicted by ChPT. Currently, no theoretical calculation incorporates these effects. Furthermore, just above threshold other p-wave multipoles start to contribute. It has been pointed out [3] that these p-wave multipoles are of great interest as key low energy tests of ChPT. We should also point out that in most of the above-threshold calculations the double scattering diagram was evaluated using the factorization approximation whereby the intermediate nucleon momenta are fixed. While this eliminates a time consuming sixfold integration the validity of the approximation is not well founded. One of the aims of this work is to investigate the model dependence of this assumption.

On the experimental side, data is now available from the Saskatchewan Accelerator Laboratory for differential and total cross sections for the coherent channel at photon lab energies from near threshold up to 160 MeV [8]. Experiments are also planned at the Mainz Microtron to measure neutral pion photoproduction on deuterium including the break-up channel.

Our paper is organized as follows. In Sec. II the formalism used for the calculation is described. First, the scattering operators including both impulse and rescattering terms are derived. Input to these equations consists of the elementary

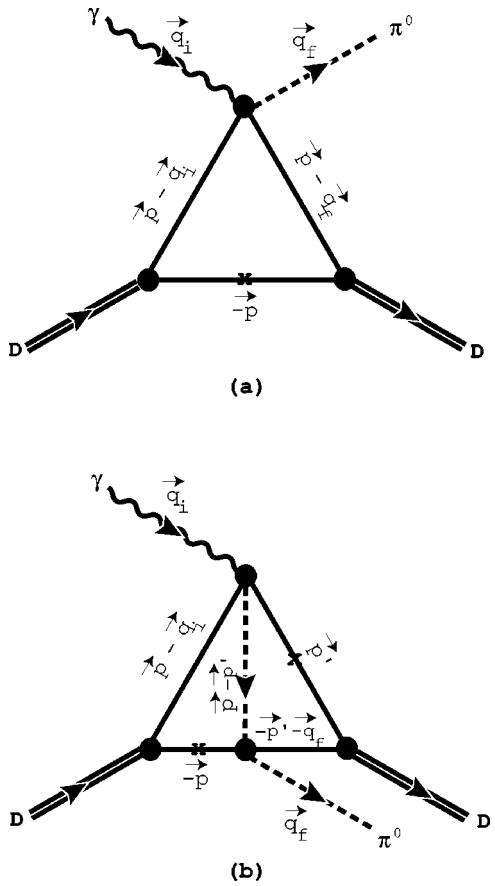

FIG. 1. Single (a) and double (b) scattering diagrams for the $\gamma + D \to \pi^0 + D$ process with all momenta defined in the γD c.m. frame.

operators for pion photoproduction and pion-nucleon scattering. These are reviewed along with the required boost relations. In Sec. III, we examine in some detail the double scattering diagram. We compare the results based on the factorization approximation, often assumed in the literature, with the numerical calculation of the sixfold integration. Section IV opens with a discussion on the threshold deuteron amplitude E_d [6] that has been recently extracted from experiment [8] along with a comparison with the recently completed ChPT calculation [6] which is strictly valid at threshold. The remainder of the section deals with the region above threshold and numerical results of the unpolarized cross section are presented and compared with experiment. A summary and conclusions are given in Sec. V.

II. FORMALISM

The reaction mechanism of the scattering amplitude for coherent neutral pion photoproduction on the deuteron is described as a sum of single and double scattering terms as illustrated in Fig. 1. The rescattering process is mediated by a pion exchanged between the two nucleons [Fig. 1(b)] and turns out to be a very important correction to the impulse approximation [Fig. 1(a)] [4]. The reason is that in the threshold region the charged pion photoproduction amplitude is an order of magnitude larger that the corresponding neutral pion production amplitude that enters the single scattering diagram. Therefore it is crucial to examine this double scattering diagram with great care before any meaningful information on the neutron amplitude can be extracted.

A. Kinematics, matrix elements, and cross section

The deuteron scattering amplitude has the following two pieces:

$$\mathcal{F}(\gamma D \to \pi^0 D) = \mathcal{F}^{\mathrm{SS}} + \mathcal{F}^{\mathrm{DS}}, \tag{1}$$

where the labels SS and DS stand for single and double scattering contributions, respectively. They are given by

$$\mathcal{F}^{\mathrm{SS}} = 2 \int C^{\mathrm{SS}} \Psi_D^{\dagger}\left(\vec{p} - \frac{\vec{q}_f}{2}\right) \mathcal{F}_{\gamma\pi}(P_{\gamma N}^{\mu}, q_i^{\mu}, q_f^{\mu}) \times \Psi_D\left(\vec{p} - \frac{\vec{q}_i}{2}\right) d\vec{p}, \tag{2}$$

$$\mathcal{F}^{\mathrm{DS}} = -2\frac{1}{(2\pi)^2} \int C^{\mathrm{DS}} \Psi_D^{\dagger}\left(\vec{p}\,' + \frac{\vec{q}_f}{2}\right) \mathcal{F}_{\pi\pi}(P_{\pi N}^{\mu}, q_m^{\mu}, q_f^{\mu}) \times \frac{2E_m}{(q_m^{02} - E_m^2 + i\epsilon)} \mathcal{F}_{\gamma\pi}(P_{\gamma N}^{\mu}, q_i^{\mu}, q_m^{\mu}) \times \Psi_D\left(\vec{p} - \frac{\vec{q}_i}{2}\right) d\vec{p}\,' d\vec{p}, \tag{3}$$

with $E_m = \sqrt{\vec{q}_m^{\,2} + M_\pi^2}$ and $M_\pi = M_{\pi^+}$, the charged pion mass. The amplitudes $\mathcal{F}_{\gamma\pi}$ and $\mathcal{F}_{\pi\pi}$ are the pion photoproduction and pion-nucleon scattering elementary operators and will be discussed in the next section. The coefficients C^{SS} and C^{DS} come from our choice of normalization of the reaction amplitude and are given by

$$C^{\mathrm{SS}} = \sqrt{\frac{\mu_{\gamma D}\mu_{\pi D}}{\mu_{\gamma N_1}\mu_{\pi_f N_1}}},$$

$$C^{\mathrm{DS}} = \sqrt{\frac{\mu_{\gamma D}\mu_{\pi D}}{\mu_{\gamma N_1}\mu_{\pi_m N_1}\mu_{\pi_m N_2}\mu_{\pi_f N_2}}}, \quad \mu_{\alpha\beta} = \frac{P_\alpha^0 P_\beta^0}{W_{\alpha\beta}}, \tag{4}$$

where N_1, N_2, π_m, and π_f label nucleon 1, 2, the propagating pion, and the outgoing pion. All relevant kinematics are shown in Fig. 1. Our expressions (2) and (3) agree with those given in Ref. [9]. The Fourier transform of the nonrelativistic deuteron wave function with suppressed spin projection quantum index is written as

$$\Psi_D(\vec{p}) = \frac{1}{\sqrt{4\pi}}\left[u_0(p) - \frac{1}{\sqrt{8}} S_{12}(\hat{p}) u_2(p)\right]\chi_M^1, \tag{5}$$

where S_{12} is the tensor operator

$$S_{12}(\hat{p}) = 3(\vec{\sigma}_1 \cdot \hat{p})(\vec{\sigma}_2 \cdot \hat{p}) - (\vec{\sigma}_1 \cdot \vec{\sigma}_2). \tag{6}$$

All calculations done in this paper use the Paris potential [10] to generate the deuteron wave functions. The S- and D-state wave functions u_0 and u_2 are related to the corresponding standard spatial ones by

$$u_l(p) = \sqrt{\frac{2}{\pi}} \int_0^\infty dr r j_l(pr) u_l(r) \tag{7}$$

subject to the normalization condition

$$\int_0^\infty [u_0(p)^2 + u_2(p)^2] \; p^2 dp = 1. \tag{8}$$

We have defined $q_i^\mu = (q_i^0, \vec{q}_i)$, $q_f^\mu = (q_f^0, \vec{q}_f)$, $P_i^\mu = (P_i^0, \vec{P}_i)$, and $P_f^\mu = (P_f^0, \vec{P}_f)$ as the four-momenta of the incoming photon, outgoing pion, the target, and the recoiling deuteron, respectively. We work in the γd center of momentum (c.m.) frame and all the external particles are on their mass shell so that $q_i^0 = |\vec{q}_i|$, $q_f^0 = \sqrt{\vec{q}_f^2 + M_{\pi^0}^2}$, $P_i^0 = \sqrt{\vec{P}_i^2 + M_d^2}$, and $P_f^0 = \sqrt{\vec{P}_f^2 + M_d^2}$. In addition E_γ denotes the incident photon lab energy and $W_{\gamma D} = W_{\pi D} = \sqrt{M_d^2 + 2M_d E_\gamma}$ is the total energy in the γd c.m. frame.

We shall now discuss the kinematics involved in each diagram using the spectator-on-mass-shell prescription [5,11] and assuming an average nucleon mass of $M_x = (M_p + M_n)/2$. For the single scattering diagram [Fig. 1(a)] the spectator nucleon indicated by a cross is on-shell with $p_2^\mu = (\sqrt{M_x^2 + \vec{p}^2}, -\vec{p})$. The active nucleon is off-shell and its four-momentum before being struck by the the photon is $p_1^\mu = (P_i^0 - p_2^0, -\vec{q}_i + \vec{p})$. Note that the relative momentum of the nucleons inside the deuteron in the initial state is $(\vec{p}_1 - \vec{p}_2)/2 = -\vec{q}_i/2 + \vec{p}$ rather than $\vec{p}$. The total four-momentum available to the γN subsystem is $P_{\gamma N}^\mu = (p_1^0 + q_i^0, \vec{p}_1 + \vec{q}_i = \vec{p})$ and its invariant mass is $s_{\gamma N} = W_{\gamma N}^2 = W_{\gamma D}^2 + M_x^2 - 2W_{\gamma D}\sqrt{M_x^2 + \vec{p}^2}$. In the double scattering diagram [Fig. 1(b)], the on-shell nucleons have four-momenta $p_2^\mu = (\sqrt{M_x^2 + \vec{p}_2^{\,2}}, -\vec{p})$ and $p_1'^\mu = (\sqrt{M_x^2 + \vec{p}_1'^{\,2}}, \vec{p}')$. The four-momenta of the off-shell nucleons are then determined through energy-momentum conservation and given by $p_1^\mu = (P_i^0 - p_2^0, -\vec{q}_i + \vec{p})$ and $p_2'^\mu = (P_f^0 - p_1'^0, -\vec{q}_f - \vec{p}')$. The expression for the pion propagator can now be rewritten as

$$q_m^{02} - E_m^2 = q_m^{02} - \vec{q}_m^{\,2} - M_\pi^2, \quad q_m^0 = W_{\gamma D} - \sqrt{\vec{p}^2 + M_x^2} - \sqrt{\vec{p}'^2 + M_x^2}, \quad \vec{q}_m = \vec{p} - \vec{p}'. \tag{9}$$

It is important to note that the pion propagator contains singularities at $q_m^0 = \pm E_m$ and a proper procedure is needed to evaluate the six-dimensional integral given by Eq. (3). This will be discussed in the Appendix. The total four-momentum available to the γN and πN subsystems are $P_{\gamma N}^\mu = (p_1^0 + q_i^0, \vec{p})$ and $P_{\pi N}^\mu = (p_2'^0 + q_f^0, -\vec{p}')$ respectively. The invariant masses are then given by $s_{\gamma N} = W_{\gamma N}^2 = W_{\gamma D}^2 + M_x^2 - 2W_{\gamma D}\sqrt{M_x^2 + \vec{p}^2}$ and $s_{\pi N} = W_{\pi N}^2 = W_{\pi D}^2 + M_x^2 - 2W_{\pi D}\sqrt{M_x^2 + \vec{p}'^2}$. Other prescriptions to determine $W_{\gamma N}$ have been discussed by Wilhelm and Arenhoevel [12] and by Breitmoser and Arenhoevel [13]. However, these authors discuss only single scattering diagrams so that the effect of the various prescriptions on double scattering diagrams is unclear.

In this paper, we shall focus only on the unpolarized cross section and compare with the available experimental data. One can now carry out the appropriate algebraic manipulations to obtain the coherent c.m. differential cross section:

$$\left(\frac{d\sigma}{d\Omega}\right)_{\text{c.m.}} = \frac{1}{3}\frac{|\vec{q}_f|}{|\vec{q}_i|} \sum_{M_f, M_i} |\mathcal{F}_{M_f, M_i}|^2, \tag{10}$$

where M_i, M_f are the initial and final magnetic quantum numbers of the deuteron [see Eq. (5)] and the photon helicity is chosen to be $\lambda = +1$. The matrix elements corresponding to $\lambda = -1$ are related to the $\lambda = +1$ by parity conservation in the following way:

$$\mathcal{F}_{M_f, M_i}(\lambda) = (-)^{1+\lambda+M_i-M_f} \mathcal{F}_{-M_f, -M_i}(-\lambda). \tag{11}$$

Furthermore, helicity conservation require that the matrix elements must vanish in the forward and backward directions unless $M_f = M_i + \lambda$. This provides an additional check on the numerical integrations.

B. Elementary operators

There are two elementary processes needed to evaluate the T matrix for coherent pion photoproduction on the deuteron, $\pi N \to \pi N$ and $\gamma N \to \pi N$. Since we are mainly concerned with the threshold region, only s- and p-wave amplitudes will be considered. This is a good approximation since, as will be described shortly, it reproduces the recent experimental data on the proton. The isospin structure of the elementary amplitudes is written in the usual form

$$\mathcal{F}_{\gamma\pi} = \mathcal{F}_{\gamma\pi}^{(+)} \delta_{b3} + \mathcal{F}_{\gamma\pi}^{(-)} \frac{1}{2}[\tau_b, \tau_3] + \mathcal{F}_{\gamma\pi}^{(0)} \tau_b, \tag{12}$$

$$\mathcal{F}_{\pi\pi} = \mathcal{F}_{\pi\pi}^{(+)} \delta_{ba} + \mathcal{F}_{\pi\pi}^{(-)} \frac{1}{2}[\tau_b, \tau_a], \tag{13}$$

where a, b label the Cartesian isospin indices of the incoming and outgoing pions, respectively, and $\vec{\tau}$ are the SU(2) Pauli matrices. Because the deuteron has $T = 0$ the relevant isospin structure of the elementary operators becomes $\mathcal{F}_{\gamma\pi} \equiv \mathcal{F}_{\gamma\pi}^{(+)}$ and $\mathcal{F}_{\pi\pi}\mathcal{F}_{\gamma\pi} \equiv \mathcal{F}_{\pi\pi}^{(+)}\mathcal{F}_{\gamma\pi}^{(+)} - 2\mathcal{F}_{\pi\pi}^{(-)}\mathcal{F}_{\gamma\pi}^{(-)}$ for the single and double scattering diagrams, respectively. The operators $\mathcal{F}_{\gamma\pi}^{(\alpha)}$ and $\mathcal{F}_{\pi\pi}^{(\alpha)}$ can be decomposed with the following general spin structure in the πN c.m. frame:

$$\mathcal{F}_{\gamma\pi}^{(\alpha)} = i\vec{\sigma} \cdot \vec{K}^{(\alpha)} + L^{(\alpha)}, \quad \mathcal{F}_{\pi\pi}^{(\alpha)} = i\vec{\sigma} \cdot \vec{M}^{(\alpha)} + N^{(\alpha)}, \tag{14}$$

with α being the isospin index $(+), (-)$, or (0) which will be suppressed from here on unless stated otherwise. The operators $\vec{K}, \vec{M}$ and L, N are related to the standard CGLN amplitudes [14] for pion photoproduction F_{1-4} and pion-nucleon scattering f_{1-2} by the following relations:

$$L = \vec{q}_f^{\,\star} \cdot (\vec{q}_i^{\,\star} \times \vec{a}^{\star}) F_2, \tag{15}$$

$$N = f_1 + \vec{q}_f^{\,\star} \cdot \vec{q}_i^{\,\star} f_2, \tag{16}$$

$$\vec{K} = (F_1 - \vec{q}_f^{\,\star} \cdot \vec{q}_i^{\,\star} F_2)\vec{a}^{\star} + \vec{q}_f^{\,\star} \cdot \vec{a}^{\star} \vec{q}_i^{\,\star} (F_2 + F_3) + \vec{q}_f^{\,\star} \cdot \vec{a}^{\star} \vec{q}_i^{\,\star} F_4, \tag{17}$$

$$\vec{M}=\vec{q}_f^{\star}\times\vec{q}_i^{\star}f_2, \tag{18}$$

where we have defined the vector $\vec{a}=\vec{\epsilon}^{\star}-\vec{q}_i^{\star}\cdot\vec{\epsilon}^{\star}\vec{q}_i^{\star}/q_i^{\star 2}$ so that the photoproduction operator is now explicitly gauge invariant. Here $\vec{\epsilon}^{\star},\vec{q}_i^{\star},\vec{q}_f^{\star}$ are the photon polarization and the initial and final relative momenta in the pion-nucleon c.m. frame. Note that at a $\gamma N\to\pi N$ vertex $\vec{q}_i$ is the photon momentum whereas at a $\pi N\to\pi N$ vertex $\vec{q}_i$ is the incident pion momentum. The superscript star is used to avoid confusion with the corresponding quantities in the γD c.m. frame. If only s- and p-partial wave amplitudes are retained one has

$$\mathcal{F}_{\gamma\pi}=i\vec{\sigma}\cdot\vec{a}^{\star}H_1+i\vec{q}_f^{\star}\cdot\vec{a}^{\star}\vec{\sigma}\cdot\vec{q}_i^{\star}\quad H_2+i\vec{q}_f^{\star}\cdot\vec{a}^{\star}\vec{\sigma}\cdot\vec{q}_f^{\star}H_3 +\vec{q}_f^{\star}\cdot(\vec{q}_i^{\star}\times\vec{a}^{\star})H_4, \tag{19}$$

$$\mathcal{F}_{\pi\pi}=i\vec{\sigma}\cdot\vec{q}_f^{\star}\times\vec{q}_i^{\star}G_1+G_2 \tag{20}$$

with

$$H_1=E_{0+}+\vec{q}_f^{\star}\cdot\vec{q}_i^{\star}p_1,\quad H_2=p_2,\quad H_3=0,\quad H_4=p_3, \tag{21}$$

$$G_1=0,\quad G_2=a_{\pi N}+b_{\pi N}\vec{q}_f^{\star}\cdot\vec{q}_i^{\star}. \tag{22}$$

The p_i are connected to the standard p-wave multipoles by $p_1=3e_{1+}+m_{1+}-m_{1-}$, $p_2=3e_{1+}-m_{1+}+m_{1-}$, $p_3=2m_{1+}+m_{1-}$. The P-wave amplitudes as defined in Ref. [3] are related to ours simply by $P_i=q_i^{\star}q_f^{\star}p_i$. The quantities $a_{\pi N}$ and $b_{\pi N}$ are the usual scattering lengths and volumes, respectively. Finally, our elementary amplitudes are normalized so that the differential cross sections in the π-nucleon c.m. frame are

$$\frac{d\sigma}{d\Omega}(\gamma N\to\pi N)=\frac{q_f^{\star}}{q_i^{\star}}|\overline{\mathcal{F}_{\gamma\pi}}|^2, \tag{23}$$

$$\frac{d\sigma}{d\Omega}(\pi N\to\pi N)=|\overline{\mathcal{F}_{\pi\pi}}|^2, \tag{24}$$

where the overbar means that we need to average over the initial and sum over the final spins.

In order to illustrate the model dependence of this calculation we use elementary production amplitudes from three theories. These are the effective Lagrangian approach (ELA) [15], chiral perturbation theory (ChPT) [3], and dispersion theory (DR) [16]. The ELA model gives the ''classical'' values for the proton and neutron amplitude alluded to in the Introduction supplemented by corrections due to resonance exchanges. DR and ChPT nearly agree in the threshold proton amplitudes, giving $E_{0+}^{p\pi^0}=-1.22$ and -1.16, respectively, which are more compatible with the measured value of -1.3 [1]. On the other hand their neutron amplitudes differ, with $E_{0+}^{n\pi^0}=1.19$ in the case of DR compared to 2.13 in the case of ChPT. For near threshold production from the deuteron the relevant quantity in the single scattering term is the isoscalar amplitude $E_{0+}^{(+)}=(E_{0+}^{p\pi^0}+E_{0+}^{n\pi^0})/2$. We should point out that previously most calculations of this sort have used the classical LET values of about ≈-1 for the isoscalar amplitude. However an inspection of Table II reveals that there are considerable differences in this amplitude as predicted by the three theories used here. This is one of the motivations for performing an accurate measurement of $D(\gamma,\pi^0)D$ near threshold. However, as we shall see, the threshold cross section is dominated by the double scattering diagram Fig. 1(b) and uncertainties in the calculation of this term may mask the $E_{0+}^{(+)}$ dependence.

TABLE I. Parameters for the s-wave multipole for various theories (see text for details). They are expressed in the standard units of $10^{-3}/M_{\pi^+}$.

	a_0		a_1		a_2	
	$p\pi^0$	$n\pi^0$	$p\pi^0$	$n\pi^0$	$p\pi^0$	$n\pi^0$
ChPT	-0.13	3.32	-4.60	-4.60	3.83	4.44
DR	-0.20	2.35	-4.60	-4.60	3.80	4.30
ELA	-1.04	1.80	-4.60	-4.60	3.74	4.25

As one moves away from threshold it is important to include the effects of p-wave multipoles as well as energy-dependence of the s-wave amplitudes. To describe the energy dependence of the proton s-wave multipole E_{0+} we use the parametrization of Ref. [17]

$$E_{0+}=a_0+a_1(W^2-W_{\rm th}^2)/(2M_NM_{\pi^0})+ia_2q_+/M_{\pi^+}. \tag{25}$$

Here $W_{\rm th}=M_N+M_{\pi^0}$ is the threshold c.m energy, q_+ is the $\pi-N$ c.m. momentum (continued to nonphysical imaginary momenta below the charged pion threshold), and a_i are energy-independent parameters. The last term is related to the rescattering of the pion before being emitted and is responsible for the cusp effect. In this low-energy region, a_2 can be well approximated by a product of the πN scattering length $a_{\pi N}$ (values used are discussed below) and the s-wave charged pion electromagnetic production amplitude E_{0+}:

$$a_2^{p\pi^0}=a_{\pi^+\pi^0}E_{0+}^{n\pi^+}M_{\pi^+},\quad a_2^{n\pi^0}=a_{\pi^-\pi^0}E_{0+}^{p\pi^-}M_{\pi^+}. \tag{26}$$

The parameter a_2 has been evaluated using the experimental scattering lengths [18] $a_{\pi^-\pi^0}=-a_{\pi^+\pi^0}=-\sqrt{2}a_{\pi N}^{(-)}$ (see below) and $\{E_{0+}^{n\pi^+},E_{0+}^{p\pi^-}\}=\{28.2,-32.7\},\{28.0,-31.7\},\{27.51,-31.28\}$ in units of $10^{-3}/M_{\pi^+}$ for ChPT, DR, and ELA, respectively. The parameter a_0 is then obtained by evaluating Eq. (25) at threshold and equating it to the threshold value of E_{0+} predicted by the theory in question. Note that the term proportional to a_1 vanishes at threshold. The parameter a_1 is determined by the experimental slope of the real part of s-wave multipole past the cusp. Note that this procedure produces different a_0 and a_2 for each of the three theories but the same a_1. Table I lists the resulting parameters for the three cases while the results of the fit are displayed in Fig. 2. Clearly, the energy dependence is well reproduced for ChPT and DR theories but not so well for the ELA model due to its large value of $E_{0+}^{p\pi^0}$ at threshold.

Given the fact that the values for a_2 are not that different for $p\pi^0$ and $n\pi^0$ channels, one might expect the same to hold for a_1. In order to make a prediction of the energy

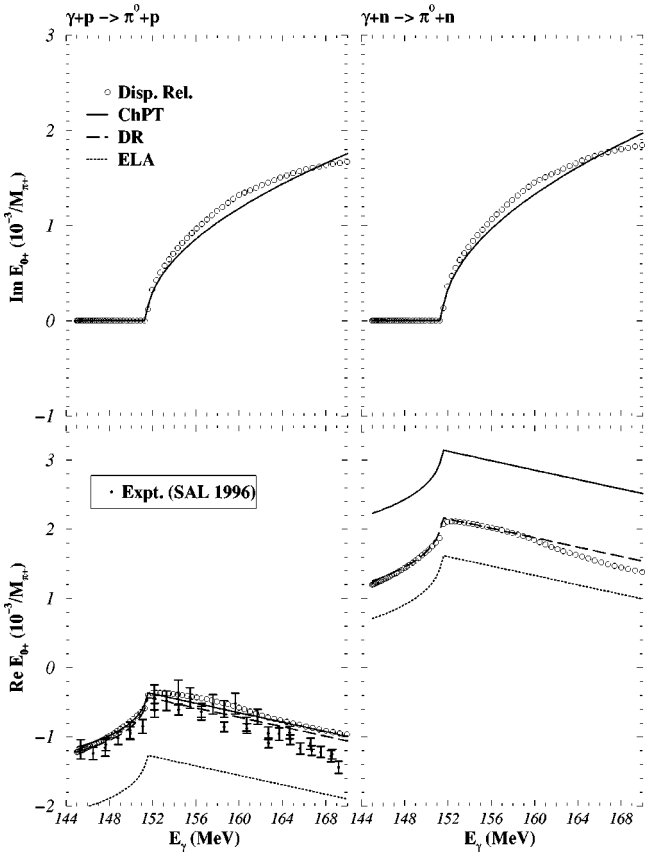

FIG. 2. Energy dependence of the s-wave multipole E_{0+} for both proton target (left pane) and predicted neutron target (right pane). The upper (lower) panel are for the imaginary (real) part of the amplitude. The data is taken from Ref. [1]. The different curves are for various theories as discussed in the text.

dependence of $E_{0+}^{n\pi^0}$ we therefore assume that a_1 is the same for both the proton and neutron target as well as for all theories. This leads to our prediction (dashed line) in Fig. 2 for the s-wave multipole for the $\gamma n \to \pi^0 n$ reaction compared to the correponding calculation of dispersion theory (empty circles) [16]. We also display the results for ChPT and ELA with solid and dotted lines, respectively. It is expected that the simple cusp function as given by Eq. (25) is in agreement with the sophisticated dispersion calculation for both neutral pion photoproduction channels. As can be seen from Fig. 2, the main difference between various theories is the threshold value, especially in the case of the neutron target. It is worth emphasizing at this point that the same a_2 enters the rescattering diagram of Fig. 1(b) involving two nucleons (two-body rescattering) and the rescattering term appearing in E_{0+} [Eq. (25)] involving only one nucleon (one-body rescattering). Therefore, the two rescattering corrections should be treated consistently.

As mentioned above, the contribution of p-wave multipoles becomes more important necessitating their inclusion as the energy increases. Table II gives the values of the isoscalar threshold multipoles for the three different theories considered in the present work. Figure 3 compares the calculated total cross section using the ChPT set with the recent experimental total cross-section data [1]. One observes excellent agreement over an energy range from threshold, corresponding to a photon lab energy of $E_\gamma = 145.7$ MeV, up to 170 MeV. Also shown by a dashed line is the prediction for the neutron target where the cusp structure is more visible. In Fig. 4, we show the corresponding angular distributions for various photon lab energies and again the agreement is very good. This figure also illustrates the importance of the energy dependence of the s-wave multipole. A constant s-wave multipole set equal to its threshold value results in the dashed curves. The importance of including the energy dependence can clearly be seen especially around the charged pion production threshold.

TABLE II. Threshold s- and p-partial wave amplitudes used in the $\gamma D \to \pi^0 D$ analysis.

Units	$E_{0+}^{(+)}$ $10^{-3}\ M_{\pi^+}^{-1}$	$p_1^{(+)}$ $10^{-3}\ M_{\pi^+}^{-3}$	$p_2^{(+)}$ $10^{-3}\ M_{\pi^+}^{-3}$	$p_3^{(+)}$ $10^{-3}\ M_{\pi^+}^{-3}$
ChPT	$+0.485$	$+8.87$	-9.68	$+11.28$
DR	-0.015	$+9.08$	-10.04	$+10.00$
ELA	-0.690	$+9.98$	-10.16	$+12.00$

Finally we discuss the parameters used to describe the πN to πN vertex. The pion-nucleon s-wave scattering lengths are obtained from a recent experiment on strong interaction shifts in pionic hydrogen [18]. Due to the smallness of the isospin even scattering lengths $a_{\pi N}^{(+)}$, there are still uncertainties surrounding its values which can range between 3 and $8\times10^{-3}/M_{\pi^+}$ [19]. Our results are not sensitive to the value of $a_{\pi N}^{(+)}$ due to its smallness as compared to $a_{\pi N}^{(-)}$. The effect of the p-wave rescattering, i.e., the contribution from scattering volumes, was shown by Koch and Woloshyn [4] to amount to less than 3% and therefore we have neglected it. Furthermore they also concluded that multiple s-wave rescatterings can be ignored since they are suppressed by the factor $a_{\pi N}\langle 1/r\rangle$. For the purpose of the present work we shall neglect all these higher order rescattering effects. We have assumed the central values of $-8.0\times10^{-3}/M_{\pi^+}$ and $96.0\times10^{-3}/M_{\pi^+}$ [18] for $a_{\pi N}^{(+)}$ and $a_{\pi N}^{(-)}$, respectively.

Finally we note that in order to use the multipoles as input

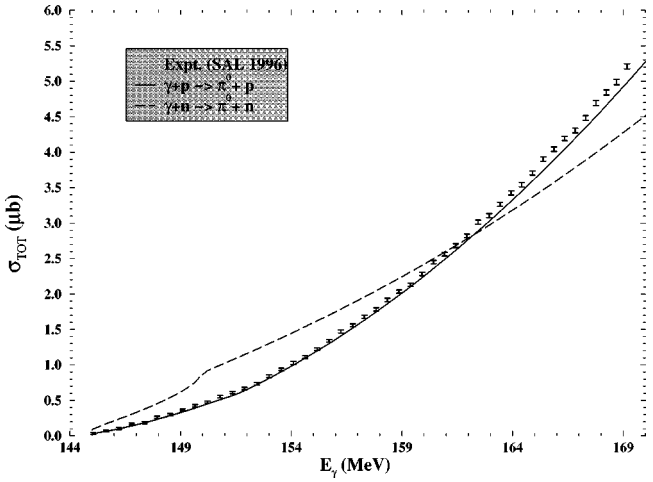

FIG. 3. Total cross section (solid curve) for $\gamma + p \to \pi^0 + p$ reaction for photon lab energies from threshold $E_\gamma = 144.66$ up to 170 MeV. The dashed curve is our prediction for $\gamma + n \to \pi^0 + n$. The experimental data are for the proton target measured at the Saskatchewan Accelerator Lab [1].

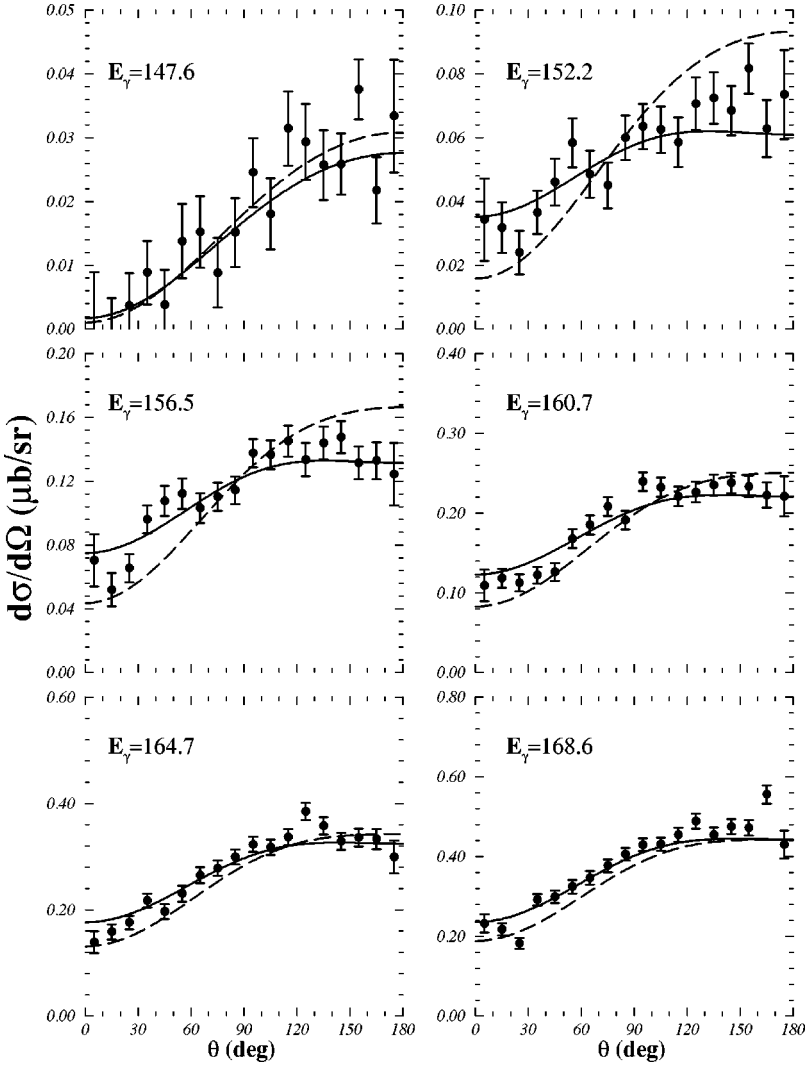

FIG. 4. Differential cross section for $\gamma+p\rightarrow\pi^0+p$ reaction for a selected set of photon lab energies. The dashed line is the result of ignoring the energy dependent cusp effect.

to the deuteron calculation, one needs to boost the elementary operators to the $\gamma-D$ c.m. frame where the observables are calculated. The relevant Lorentz transformations are

$$\vec{q}_i^{\star}=\vec{q}_i+f_i\vec{P}_{\gamma N}, \tag{27}$$

$$\vec{q}_f^{\star}=\vec{q}_f+f_f\vec{P}_{\gamma N}, \tag{28}$$

$$\vec{a}^{\star}=\vec{\epsilon}+(\vec{\epsilon}\cdot\vec{P}_{\gamma N}/W_{\gamma N})[\vec{q}_i^{\star}/q_i^{0\star}+\vec{P}_{\gamma N}/(P^0_{\gamma N}+W_{\gamma N})], \tag{29}$$

$$f_i=\left(\frac{\vec{q}_i\cdot\vec{P}_{\gamma N}}{(P^0_{\gamma N}+W_{\gamma N})}-q_i^0\right)/W_{\gamma N}, \tag{30}$$

$$f_f=\left(\frac{\vec{q}_f\cdot\vec{P}_{\gamma N}}{(P^0_{\gamma N}+W_{\gamma N})}-q_f^0\right)/W_{\gamma N}, \tag{31}$$

$$q_i^{0\star}=(q_i^0P^0_{\gamma N}-\vec{q}_i\cdot\vec{P}_{\gamma N})/W_{\gamma N}. \tag{32}$$

Similar expressions can be obtained for the relative momenta in the $\pi N\rightarrow\pi N$ channel with the obvious replacement $P^{\mu}_{\gamma N}\rightarrow P^{\mu}_{\pi N}$.

III. EFFECTS OF FERMI MOTION IN THE PION PROPAGATOR

Written out explicitly the denominator of the DS term in Eq. (3) is

$$D=q_m^{02}-E_m^2=[W_{\gamma D}-\sqrt{\vec{p}^2+M_x^2}-\sqrt{\vec{p}'^2+M_x^2}]^2-(\vec{p}-\vec{p}')^2-M_\pi^2+i\epsilon. \tag{33}$$

This denominator requires an evaluation of six-dimensional integrals over $d\vec{p}d\vec{p}'$. The numerical method adopted for this is discussed in the Appendix. Here we want to compare the direct evaluation of this integral (referred to as exact) to approximations used by others which reduce the dimensionality of the integral. These approximations basically amount to various approximations for the nucleon kinetic energy in D. The further neglect of momentum dependence of the operators and/or the use of simplified deuteron wave functions allows some of the integrations to be done analytically. Thus Lazard *et al.* [20] in one case simply set these kinetic energies to zero. We refer to this as case 1. In another approximation which we refer to as case 2 Lazard *et al.* [20] and more recently by Garcilazo *et al.* [11] considered the following replacement:

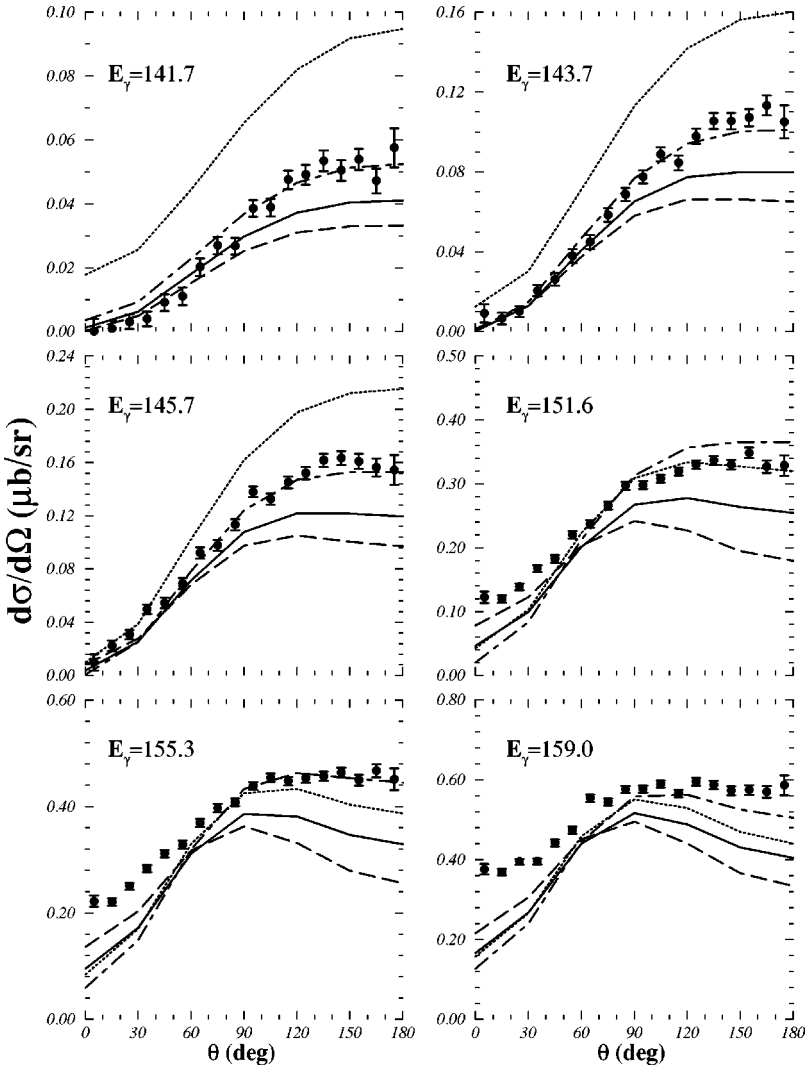

FIG. 5. Sensitivity of the differential cross section $\gamma + D \to \pi^0 + D$ to the treatment of the pion propagation for various photon lab energies. The data is from the Saskatchewan Accelerator Lab [8]. The curves correspond to the ChPT set for the elementary mulipoles with solid (exact), dotted (case 1), dash dot (case 2), dashed (case 3).

$$\sqrt{\vec{p}^2 + M_x^2} + \sqrt{\vec{p}'^2 + M_x^2} \to \sqrt{\frac{1}{4}\vec{q}_i^2 + M_x^2} + \sqrt{\frac{1}{4}\vec{q}_f^2 + M_x^2}. \tag{34}$$

We denote as case 3 the approximation used by Koch and Woloshyn [4] and more recently by Tiator, Bennhold, and Kamalov [21] where both p and p' are replaced by $p_{\rm eff} = 150$ MeV. Using the ChPT set of the elementary amplitudes (see Tables I and II), the results of these various approximations are displayed and compared with the data [8] in Fig. 5. One observes that cases 1 and 2 consistently give a larger cross section at larger angles, especially near threshold energies. It is interesting to see that case 2 reproduces the data rather well for the three lowest energies. As will be discussed in Sec. IV, the data for the three lowest energies can also be described using the exact treatment and the DR set for the amplitudes. This indicates that a proper treatment of the pion propagation is necessary in order to extract reliably the neutron amplitude. Case 3, on the other hand, lies above the exact curve at small angles and then falls below it at larger angles, except at the lowest energy where it is below the exact curve for all angles. Thus the calculated cross section is sensitive to the method of treating the denominator in the DS integral, an observation made earlier by Fäldt [22]. All results given later in this paper use the exact treatment of this term.

The approximations in cases 1, 2, and 3 above are all based on assuming that the kinetic energies of the nucleons appearing in D can be replaced by some effective values. If, as a further approximation, the elementary scattering operators are assumed to be independent of Fermi momenta then the resulting approximation is referred to as a factorization approximation. This approximation allows the amplitude to be written as

$$\begin{aligned}\mathcal{F}_{\gamma D} = {} & 2C_s \int \Psi_d^\dagger(\vec{r}) \mathcal{F}_{\gamma\pi}^{(+)} \Psi_d(\vec{r}) e^{i\vec{r}\cdot\vec{t}_m/2} d^3\vec{r} \\ & + 2C_s C_d \int \Psi_d^\dagger(\vec{r}) \cdot (\mathcal{F}_{\pi\pi}^{(+)} \mathcal{F}_{\gamma\pi}^{(+)} \\ & - 2\mathcal{F}_{\pi\pi}^{(-)} \mathcal{F}_{\gamma\pi}^{(-)}) \Psi_d(\vec{r}) f(r) e^{i\vec{r}\cdot\vec{t}_p/2} d^3\vec{r}. \end{aligned} \tag{35}$$

Here $\Psi_d(\vec{r})$ is the deuteron wave function in coordinate space, $t_m = \vec{q}_i - \vec{q}_f$ is the momentum transfer to the deuteron, and $t_p = \vec{q}_i + \vec{q}_f$. The function $f(r)$ is defined as

$$f(r)=\begin{cases} e^{iq_{\rm eff}r}/r & q_{\rm eff}^2>0 \\ e^{-|q_{\rm eff}|r}/r & q_{\rm eff}^2<0, \end{cases} \tag{36}$$

where $q_{\rm eff}^2=q_m^{02}-M_\pi^2$. The remaining kinematical quantities are

$$C_s=\frac{W_{\gamma N}}{W_{\gamma D}}\sqrt{\frac{E_D(\vec{q}_i)E_D(\vec{q}_f)}{E_N(\vec{q}_i/2)E_N(\vec{q}_f/2)}},$$

$$C_d=\frac{W_{\pi N}}{\sqrt{E_N(\vec{q}_i/2)E_N(\vec{q}_f/2)}} \tag{37}$$

with $W_{\gamma D}=W_{\pi D}=E_\gamma(\vec{q}_i)+E_D(\vec{q}_i)$ and

$$W_{\gamma N}^2=W_{\gamma D}^2+M_N^2-2W_{\gamma D}\sqrt{M_N^2+q_i^2/4}, \tag{38}$$

$$W_{\pi N}^2=W_{\pi D}^2+M_N^2-2W_{\pi D}\sqrt{M_N^2+q_f^2/4}. \tag{39}$$

We have used these approximations mainly as checks on the accuracy of the multidimensional momentum space integrations.

IV. RESULTS AND DISCUSSIONS

A. Threshold

Reference [6] quantifies the threshold cross section by the number E_d defined through

$$E_d^2=\frac{3}{8}\frac{|\vec{q}_i|\,d\sigma}{|\vec{q}_f|d\Omega}\bigg|_{\vec{q}_f|\to 0}. \tag{40}$$

A recently measured value for this is $E_d=-1.45\pm0.09$ [8] in the standard units of $10^{-3}/M_{\pi^+}$. In the case of a pure s-wave deuteron we can relate, ignoring boost effects, a single matrix element $\mathcal{F}_{M_f,M_i}$ to E_d by

$$E_d=\frac{i}{2}\mathcal{F}_{0,-1}=\frac{i}{2}\mathcal{F}_{1,0}. \tag{41}$$

We note that the equality $\mathcal{F}_{0,-1}=\mathcal{F}_{1,0}$ no longer holds if the deuteron D state is added and there are nucleon momentum terms arising from the Lorentz boost. Nevertheless a reasonable understanding of the main physics determining E_d can be obtained by looking at a pure s-wave deuteron. Our s-wave deuteron results are simply obtained by turning off the d-wave in the wave function, i.e., we *do not renormalize* the s wave to unity. We consider then the SS and DS contributions to E_d.

In the case of the SS contribution to E_d one could delineate the various effects which determine its value. These would include (1) the energy dependence of $E_{0+}^{(+)}$, (2) the p-wave contributions induced by the Lorentz boost, (3) the treatment of $W_{\gamma N}$ in the boost factors Eqs. (30)–(33), and (4) the influence of the deuteron D state. We leave this degree of detail to a later paper and for now just summarize the main effects. Clearly the value of $E_{0+}^{(+)}$ is crucial for the SS term. However, so also is the effect of the Lorentz boost. Thus if we use energy-independent values of $E_{0+}^{(+)}$ as given in Table II then E_d for the ChPT parameters goes from $+0.375$ (no boost) to $+0.246$ (boost on). Similarly the DR parameters give E_d from -0.012 (no boost) to -0.144. The magnitude of the boost effect is similar to that found in Refs. [4] and [22]. Notice again the opposite signs between the ChPT and DR values of the SS contribution to E_d caused by their very different predictions for $E_{0+}^{n\pi^0}$. If one next incorporates both the energy dependence and the boost into $E_{0+}^{(+)}$, then the values for E_d become 0.145 and -0.235 for ChPT and DR, respectively. We shall see that although the DS term dominates the value of E_d, these two different SS contributions will lead to an overall difference of about 25% in their predictions of E_d.

TABLE III. Effect of Fermi motion on $|E_d|$ for ChPT and DR parameter sets.

Case	ChPT	DR
Exact	1.25	1.63
1	2.41	2.79
2	1.51	1.88
3	1.05	1.43

Apart from its sensitivity to the method of treating Fermi motion the DS term depends nearly linearly on the $a_{\pi N}^{(-)}$ π-N scattering length due to the relatively small contribution of the π^0-N and p-wave rescattering processes. Both ChPT and DR predict nearly the same values for charged meson production so that they yield (s-wave deuteron) the same value of -1.28 for the DS contribution to E_d. Adding the SS and DS contributions together we obtain the s-wave deuteron values for E_d of -1.14 for ChPT and -1.52 for DR.

Finally our complete calculation of E_d results from turning on the deuteron d state and incorporating the energy dependence of $E_{0+}^{(+)}$. Table III displays these results for the ChPT and DR parameter sets as a function of the technique employed for treating Fermi motion in the rescattering term. Note that what we have actually calculated in this table is $|E_d|=\sqrt{\Sigma_{M_f,M_i}|\mathcal{F}_{M_f,M_i}|^2}/2$. As mentioned previously the threshold cross section is not determined by a single matrix element when both the D-state and Lorentz boost terms are present. Not surprisingly the results are consistent with the 141.7 MeV cross section shown in Fig. 5, i.e., that case 3 is the lowest and case 1 is the largest. The important observation is that the approximately 30–40 % difference between the ChPT and DR sets is due solely to their disparate values of $E_{0+}^{n\pi^0}$. Beane *et al.* [6] calculate $E_d=-1.8\pm0.2$ using chiral perturbation theory for the kernel sandwiched between phenomenological deuteron wave functions. Our single scattering contribution is similar to theirs with the following exceptions: (i) they do not incorporate energy dependence into $E_{0^+}^{(+)}$ and (ii) their estimation of the effect of the Lorentz boost appears to disagree with ours and that of others [4,22]. However, we can reproduce the value of their single scattering contribution to E_d. The double scattering (labeled three-body contribution in Beane *et al.* [6]) contribution as calculated by us is phenomenological based on the works in Refs. [4,5,22,9,11]. Beane *et al.* [6] have calculated all diagrams to

order four in small momenta with all possible insertions obtained from the chiral Lagrangian in the heavy baryon formalism. Their main contribution, diagram Fig. 1(b) with vertices from the leading order $\pi - N$ Lagrangian, gives a value of -2.2 for E_d (for S-wave deuteron wave function). The next correction is similar to the diagram in Fig. 1(b) except that the incident photon is absorbed by the propagating pion. It only contributes $+0.43$ to E_d. The rest of their diagrams which encompass $1/M_N$ corrections are about 10% of the main contribution. Their treatment of Fermi motion seems to follow case 1 (see discussion in previous section) and it is unclear to us how such an approximation can be valid given that a proper treatment of Fermi motion reduces the double scattering contribution by almost 50%.

B. Above threshold

Since photoproduction experiments are done above threshold it follows that any threshold information such as the quantity E_d discussed above relies heavily on the extrapolation of the data above threshold. This region just above threshold is sensitive to other p-wave mulipoles and a consistent discription of the low-energy coherent neutral pion photoproduction on the deuteron must also include the energy range in the vicinity of the threshold. We recall in particular that $p_2^{(+)}$ and $p_3^{(+)}$ which do not enter the threshold results do, however, contribute above threshold. Therefore reproducing threshold parameters does not necessarily mean that the observables can be described adequately. Before we compare our predictions with the recent experimental data, we wish to recall, as discussed in Sec. III, that a proper treatment of the pion propagation in the double scattering diagram is necessary. As shown in the Appendix, the evaluation of the double scattering contribution can be greatly simplified if the nucleons kinetic energies are assumed constant, i.e., ignore their Fermi motion. In what follows we shall not make such a simplification and consider the Fermi effects fully. First, the sensitivity to the deuteron d-state component of the wave function is examined. Figure 6 depicts the reduced differential cross sections at three photon energies of 140,150,160 MeV with (solid line) and without (dotted line) the d-state component. We remark that the s state only curve is the contribution from the the s state which is 94.2% of the Paris deuteron wave function. The solid curve results when the remaining 5.8% of the wave function, i.e., the d wave, is added in. The effects are unremarkable for the 150 and 160 MeV distributions. However, for the near threshold curve at 140 MeV the effects of the small d wave are indeed sizable. This was observed in the previous section where E_d was calculated in an s wave only model and later the complete model. Closer inspection shows that this sensitivity disappears if the Lorentz boost is turned off.

We now come to the comparison of the calculation with the recent experiment just completed at the Saskatchewan Accelerator Laboratory. Since only π^0 were detected, the actual process includes both the coherent and breakup channels, i.e., $D(\gamma,\pi^0)X$. The data shown in Figs. 7 and 8 are extracted based on a simple theoretical model for the breakup channel, i.e., $D(\gamma,\pi^0)np$ (see Ref. [8] for details). We remark that the breakup channel should have no effects at the very low photon lab energies, in particular the 141.7

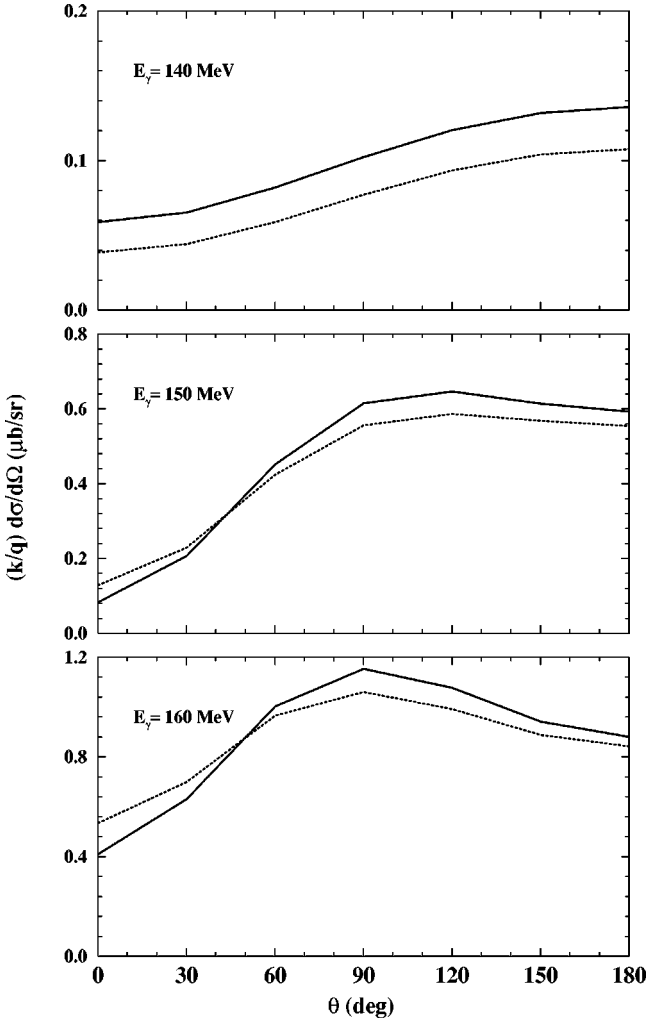

FIG. 6. Predicted differential cross section for $\gamma + D \to \pi^0 + D$ showing the effect of the D-state deuteron bound state wave function. The dashed curve results from turning off the D-state component of the wave function (without renormalizing).

and 143.7 MeV points should be less contaminated by the breakup channel. A careful treatment of the breakup channel would help ascertain the reliability of the theoretical estimates as calculated in Ref. [8]. With these cautionary remarks on the experimental data we display in Fig. 7 the angular distributions at some selected energies for the three theories discussed in Sec. II B. The ELA and DR are shown by dotted and dashed curves respectively while the ChPT curve is indicated with a thin solid line. The thick solid line is obtained by using the ChPT values but with the p-wave multipoles $p_1^{(+)}, p_2^{(+)}$ multiplied by a factor of 1.3 as suggested in Ref. [8]. It is remarkable that such a scaling reproduces the data across the full energy range while all other curves fail to do so. If such a scaling were indeed a fact, it would be difficult to understand since it would imply a drastic change of the amplitudes $p_1^{(+)}, p_2^{(+)}$ from currently accepted values. That is, as can be seen from Table II the various theories agree to within 5% on these amplitudes. Another observation is that DR seem to reproduce the three low energies rather well which raises the question of whether the breakup channel is underestimated in Ref. [8]. This un-

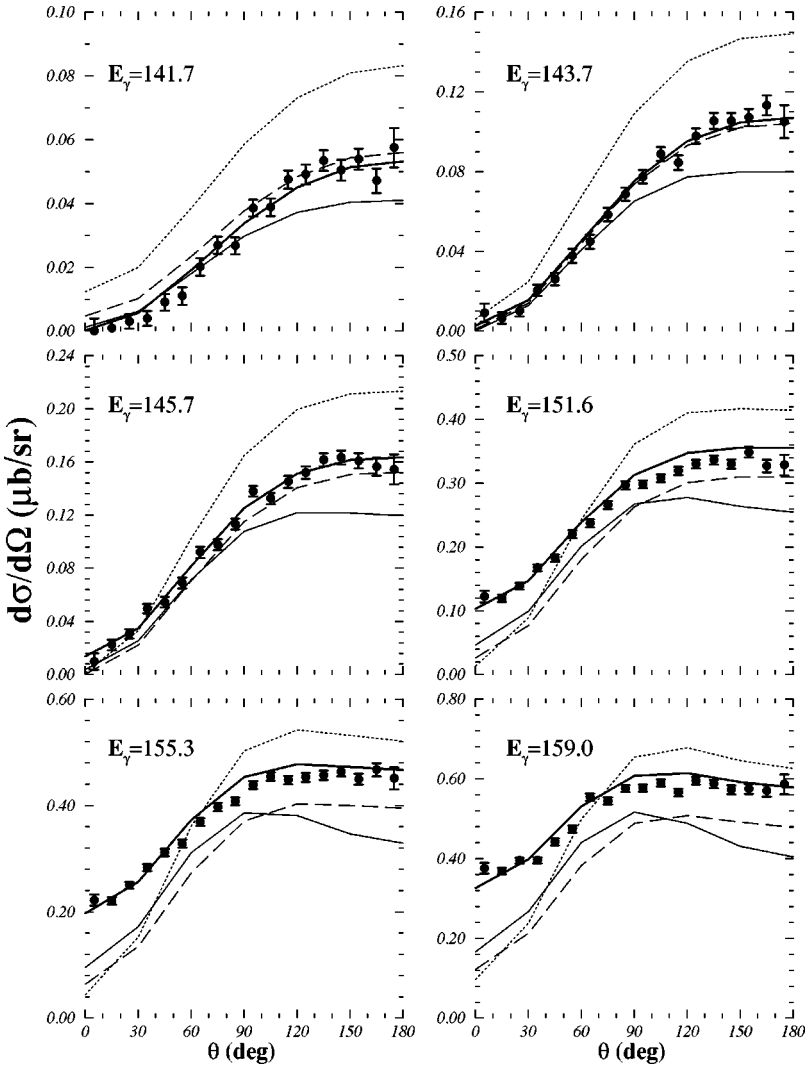

FIG. 7. Predicted differential cross section as compared with the very recent data from the Saskatchewan Accelerator Lab [8]. The curves correspond to various sets of values for the elementary multipoles (see Table II): Thin solid (ChPT), dashed (DR), dotted (ELA). The thick solid line is obtained by multiplying ChPT values for $p_1^{(+)}, p_2^{(+)}$ by 1.3.

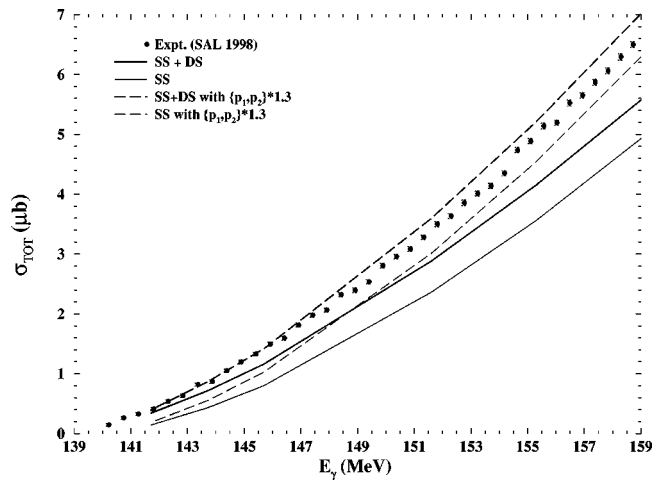

FIG. 8. Predicted total cross section for $\gamma + D \to \pi^0 + D$ reaction as compared with the experiment [8]. The thick and thin lines represent the total (single + double) and single scattering contributions, respectively, based on ChPT values for the elementary amplitudes. The dashed lines are obtained with $p_1^{(+)}, p_2^{(+)}$ multiplied by 1.3.

derscores the need, as mentioned above, for a full calculation of the $\gamma D \to \pi^0 np$ reaction.

It is useful to recall that the difference among different theories ELA, DR, and ChPT is connected with the $E_{0+}^{(+)}$ amplitude since their predictions of all the other remaining mutiploles are within a few percent (see Table II). Therefore the sensitivity seen in Fig. 7 can be ascribed to the different neutron amplitude used. For example, if we fixed the proton amplitude $E_{0+}^{p\pi^0}$ to the experimental value of roughly -1.3 then using Table II one obtains for $E_{0+}^{n\pi^0}$ amplitude 2.27,1.27,-0.08 for ChPT, DR, and ELA, repectively. Finally, in Fig. 8 we show the computed total cross section by thick solid (thick dashed) curves for the ChPT parameter set only without (with) $p_1^{(+)}, p_2^{(+)}$ scaled as in Fig. 7. Here we show the magnitude of the single scattering (SS) diagram with the corresponding thin curves. The scaled total, single scattering (SS) and double scattering (DS), seem to be in agreement with the extracted data with slight deviation at the high energy end. Obviously, the nonscaled curve does not come as close to the data.

V. CONCLUSIONS

Coherent π^0 photoproduction on the deuteron has been studied including rescattering effects. The Fermi motion has

been taken into account fully without making use of the so-called factorization approximation or frozen nucleon approximation. For the elementary reactions, we have assumed that the process is dominated by only the lowest partial s- and p- wave amplitudes. The reaction on the proton target $\gamma p \to \pi p$ is well described and compares very well with the latest data for the total and differential cross sections [1]. To study the sensitivity to the neutron amplitude we have chosen three theories where the values for the neutron s-wave multipole are calculated to be 0.4 (ELA), 1.19 (DR), and 2.13 (ChPT), respectively. Our findings can be summarized as follows. (i) The effects of the kinetic energies of the nucleons in the pion propagator are found to be sizeable even at threshold. (ii) The D-state mixture in the deuteron bound state wavefunction has also been examined and shown to affect mainly the near threshold region because of the Lorentz boost. (iii) The results seem to be very sensitive to the value of the s-wave neutron amplitude $E_{0+}^{n\pi^0}$. We have compared our results with the very recent extracted experimental [8] data and found that in order to reproduce the data one needs to increase the values of the p-wave multipoles $p_1^{(+)}, p_2^{(+)}$ by roughly 30%. This is in major disagreement with the current accepted values for these amplitudes. However, one should realize that the experimental data on the coherent process is based on a simple theoretical model for the breakup channel. Such a theoretical calculation for the breakup channel needs to be refined before any definite statements can be made. One expects the effects of the breakup channel to increase in importance with the energy. Such a calculation may also help resolve the question of why the three low-energy data sets below 150 MeV appear to be more consistent with DR than with the other two theories examined in this work.

Next, before any reliable statements can be made about the neutron amplitude, one needs to further refine the calculation by examining the importance of off-shell effects and estimate reliably the size of higher order rescattering processes. On the experimental side, we need to separate the coherent and the incoherent production on the deuteron in order to be able to extract the neutron amplitude in an unambigious way. Furthermore any polarization data would provide valuable information that may help sort out the importance of the smaller imaginary part of the amplitude.

ACKNOWLEDGMENTS

This work has been supported by the Natural Sciences and Engineering Research Council of Canada. We wish to thank Jack Bergstrom for providing us with the experimental data and Ru Igarashi for his assistance in the preparation of the figures. M.B. is grateful to Sabit Kamalov and Lothar Tiator for many stimulating communications.

APPENDIX: THE DOUBLE SCATTERING DIAGRAM

As mentioned earlier, the rescattering diagram develops poles at $q_m^0 = \pm\sqrt{\vec{q}_m^{\,2} + M_\pi^2}$ which implies that the scattering amplitude becomes complex. The imaginary part of the scattering amplitude $\mathcal{F}^{\rm DS}$ has been ignored so far in all near-threshold coherent π^0 photoproduction calculations on deuterium. In order to evaluate the six-dimensional integral we assume a nonrelativistic nucleon energy which is a very reasonable approximation since most of the contribution to the integral comes from the region where the diffrence between relativistic and nonrelativistic nucleon energy is less than a percent. In this case, after a suitable change of the integration variables in Eq. (3), one is lead to evaluate an integral of the following form:

$$\mathcal{F}^{\rm DS} = \int d\vec{q}_1 \int d\vec{q}_2 \frac{F(\vec{q}_1, \vec{q}_2)}{(Aq_2^4 + Bq_2^2 + C)}, \tag{A1}$$

with $\vec{q}_1 = (\vec{p}\,' + \vec{p})/2$ and $\vec{q}_2 = (\vec{p}\,' - \vec{p})$ and $F(\vec{q}_1, \vec{q}_2)$ can be obtained from Eq. (3). We have also introduced new functions which depend only on the variable q_1 and are given by

$$A = \frac{1}{16M_x^2}, \quad B = \frac{1}{2M_x^2}(q_1^2 - W_{\gamma D} M_x),$$

$$C = \frac{1}{M_x^2}\{[q_1^2 - M_x(W_{\gamma D} - 2M_x)]^2 - M_x^2 M_\pi^2\}. \tag{A2}$$

The existence and location of the poles depend on the integration variable q_1. There are four poles but two are the image of the other two. The denominator of Eq. (A1) can be rewritten as

$$D = A(u_1^2 - q_2^2)(u_2^2 - q_2^2), \quad u_1^2 = -\frac{B + \sqrt{\Delta}}{2A},$$

$$u_2^2 = -\frac{B - \sqrt{\Delta}}{2A}. \tag{A3}$$

The poles are located on the real axis provided the discriminant $\Delta = B^2 - 4AC$ and u_1^2, u_2^2 are positive. The root u_2 is outside the range of integration and therefore causes no problem. The other pole located at $q_2 = u_1$ is treated by introducing a subtraction function which is analytically integrable and has the same behavior near the pole as the original integrand. Using the identities

$$\frac{1}{(u_1^2 - q_2^2 + i\epsilon)} = -\frac{i\pi}{2u_1}\delta(u_1 - q_2) + P\frac{1}{(u_1^2 - q_2^2)},$$

$$P\int_0^\infty \frac{dq_2}{(u_1^2 - q_2^2)} = 0, \tag{A4}$$

the integral $\mathcal{F}^{\rm DS}$ is transformed into

$$\mathcal{F}^{\rm DS} = -\frac{i\pi}{2}\int q_1^2 dq_1 u_1 G(q_1, u_1) + P\int q_1^2 dq_1 \int dq_2 \frac{q_2^2 G(q_1, q_2) - u_1^2 G(q_1, u_1)}{(u_1^2 - q_2^2)}, \tag{A5}$$

where P stands for the principal value. The function G is defined by

$$G(q_1, q_2) = \int d\Omega_{\vec{q}_1} d\Omega_{\vec{q}_2} \frac{F(\vec{q}_1, \vec{q}_2)}{A(u_2^2 - q_2^2)}. \tag{A6}$$

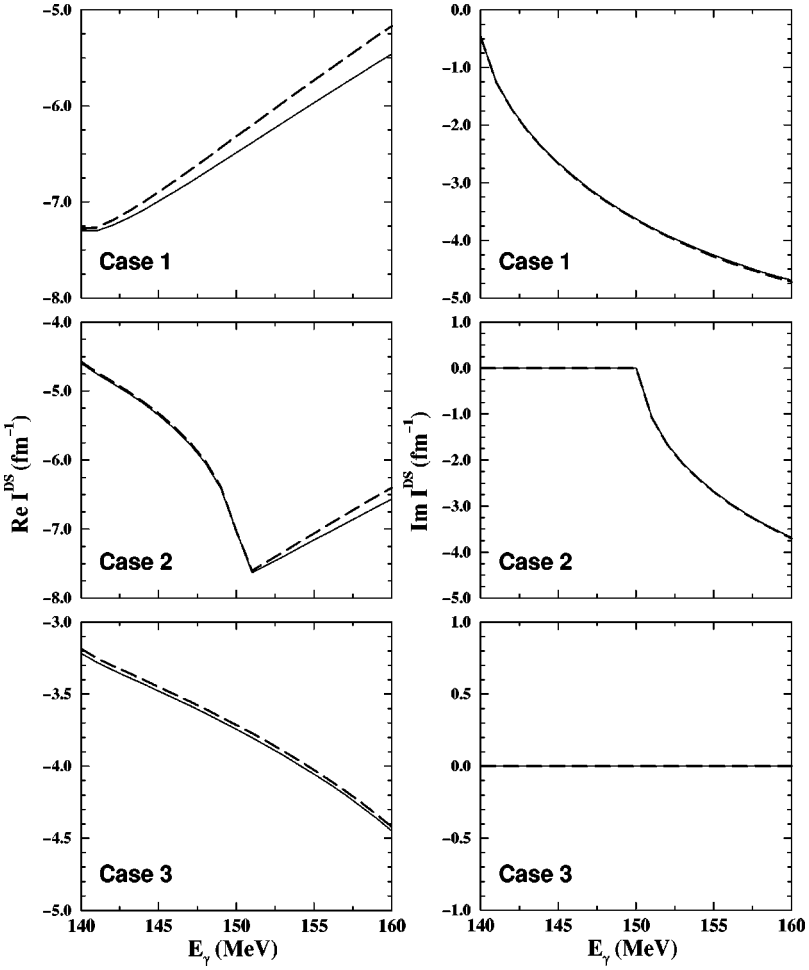

FIG. 9. P-space (solid line) vs R-space (dashed-line) for the double scattering integral Eq. (A7).

The integrals, Eqs. (A5),(A6), are performed using Gauss-Legendre quadrature with 15 points for the q_1, q_2 integrations and 9 points for the angular integrations $\Omega_{\vec{q}_1}, \Omega_{\vec{q}_2}$. As a check of our integration routine, we retained in $F(\vec{q}_1, \vec{q}_2)$ only the deuteron S-state wave function and ignored the elementary transition operators and the D-state wave function. The results for the double scattering integral are illustrated in Fig. 9 where we compare the momentum (p space) (solid line) and coordinate (R space) space (dashed line) integrations for the simplified case where $D = q_f^2 - q_2^2$. Only in this special case can one reduce the p space to r space integrations. The quantity that is compared in the figure is

$$I^{\mathrm{DS}} = \frac{1}{4\pi} \int \frac{u_0(|\vec{q}_1 + (\vec{q}_2 + \vec{q}_f)/2|)\, u_0(|\vec{q}_1 - (\vec{q}_2 + \vec{q}_i)/2|)}{(q_f^2 - q_2^2 + i\epsilon)} \times d\vec{q}_1 d\vec{q}_2 . \tag{A7}$$

[1] J. Bergstrom *et al.*, Phys. Rev. C **53**, R1052 (1996).
[2] M. Fuchs *et al.*, Phys. Lett. B **368**, 185 (1996).
[3] V. Bernard, N. Kaiser, and U.-G. Meißner, Z. Phys. C **70**, 483 (1996); V. Bernard, N. Kaiser, and U.-G. Meißner, Phys. Lett. B **378**, 337 (1996); for a review see V. Bernard, N. Kaiser, and U.-G. Meißner, Int. J. Mod. Phys. E **4**, 193 (1995).
[4] J.H. Koch and R.M. Woloshyn, Phys. Rev. C **16**, 1968 (1977).
[5] P. Bosted and J.M. Laget, Nucl. Phys. **A296**, 413 (1978).
[6] S.R. Beane, C.Y. Lee, and U. van Kolck, Phys. Rev. C **52**, 2914 (1995); S.R. Beane, V. Bernard, T.-S.H. Lee, Ulf-G Meißner, and U. van Kolck, Nucl. Phys. **A618**, 381 (1997).
[7] G. Fäldt, Nucl. Phys. **A333**, 357 (1980).
[8] J. Bergstrom *et al.*, Phys. Rev. C **57**, 3203 (1998); (private communication).
[9] I.V. Stoletnĭi and M.P. Rekalo, Sov. J. Nucl. Phys. **55**, 1338 (1992).
[10] M. Lacombe, B. Loiseau, J.M. Richard, R. Vinh Mau, J. Cote, P. Pires, and R. deTourreil, Phys. Rev. C **21**, 861 (1980).
[11] H. Garcilazo and E. Moya de Guerra, Phys. Rev. C **52**, 49 (1995).
[12] P. Wilhelm and H. Arenhövel, Nucl. Phys. **A593**, 435 (1995).
[13] E. Breitmoser and H. Arenhövel, Nucl. Phys. **A512**, 321 (1997).
[14] G.F. Chew, M.L. Goldberger, F.E. Low, and Y. Nambu, Phys. Rev. **106**, 1337 (1957); **106**, 1345 (1957).
[15] R.M. Davidson and N.C. Mukhopadhyay, Phys. Rev. Lett. **60**, 748 (1988); M. Benmerrouche, R.M. Davidson, and N.C. Mukhopadhyay, Phys. Rev. C **39**, 2339 (1989); R.M. David-

son, N.C. Mukhopadhyay, and R.S. Whittman, Phys. Rev. D **43**, 71 (1991).
[16] O. Hanstein, D. Drechsel, and L. Tiator, Phys. Lett. B **399**, 13 (1997).
[17] A.M. Bernstein *et al.*, Phys. Rev. C **55**, 1509 (1997).
[18] D. Sigg *et al.*, Nucl. Phys. **A609**, 269 (1996); **A617**, 526(E) (1997).
[19] S.R. Beane, V. Bernard, T.-S.H. Lee, and Ulf-G Meißner, nucl-th/9708035.
[20] C. Lazard, R.J. Lombard, and Z. Maric, Nucl. Phys. **A271**, 317 (1976).
[21] L. Tiator, C. Bennohold, and S.S. Kamalov, Phys. Rev. C **55**, 98 (1997); S.S. Kamalov (private communication).
[22] G. Fäldt, Phys. Scr. **22**, 5 (1980).